remote sensing

MDPI

Communication

Real Valued MUSIC Method for Height Measurement of Meter Wave Polarimetric MIMO Radar Based on Matrix Reconstruction

Guimei Zheng *, Chen Chen and Yuwei Song

Air and Missile Defense College, Air Force Engineering University, Xi'an 710051, China
* Correspondence: zheng-gm@163.com

Abstract: Combining the advantages of diversity provided by polarization MIMO radar and good decoherence ability of matrix reconstruction technology, a method for height measurements based on matrix reconstruction after real valued processing is developed. To solve height measurement problem in meter wave polarization MIMO radar, we first derive the corresponding flat ground signal model; then, the received data matrix is reconstructed to eliminate the influence of multipath coherent signal on height measurements. Then, the reconstructed data matrix is transformed into a real valued matrix using a unitary matrix. In order to reduce the influence of noise on the signal subspace and reduce the data dimension, singular value decomposition technology is applied to receive the signal data. Finally, the elevation and height of the target are estimated according to the principle that the signal subspace is orthogonal to the noise subspace. The proposed method does not require prior knowledge, such as the reflection coefficient, wave path difference and polarization information. Simulation experiments show that the proposed algorithm has better estimation performance and less computational complexity than conventional algorithms.

Keywords: height measurement; meter wave polarimetric MIMO radar; MUSIC; matrix reconstruction

Citation: Zheng, G.; Chen, C.; Song, Y. Real Valued MUSIC Method for Height Measurement of Meter Wave Polarimetric MIMO Radar Based on Matrix Reconstruction. *Remote Sens.* **2022**, *14*, 4121. https://doi.org/10.3390/rs14164121

Academic Editors: Fangqing Wen, Jin He, Veerendra Dakulagi and Wei Liu

Received: 11 July 2022
Accepted: 15 August 2022
Published: 22 August 2022

1. Introduction

Most existing radars are single-polarization array radars, such as MIMO radar, which can only receive one type of polarization information [1–3] of the electromagnetic wave signal. The vector sensor radar, namely the polarization radar, has polarization diversity characteristics and can obtain at least two types of polarization information or up to six types of polarization information [4–10] of the electromagnetic wave signal. Refs. [4–7] studied the angle estimation of the specially separated electromagnetic vector sensor array, and showed that the polarization information can improve the performance of angle estimation.

Refs. [8–10] studied the array popularity of large electric dipoles and magnetic loops and proposed corresponding angle and polarization estimation algorithms. It is well known that direction of arrival (DOA) estimation is an important part of array signal processing [11,12], in particular the height measurement of low altitude targets, which is affected by multipath and is difficult to measure accurately [13–18]. Severe multipath coherence signals exist in the low-elevation areas, which seriously affects the height measurement accuracy.

Therefore, polarimetric MIMO radar with both spatial diversity and polarization diversity has attracted the attention of many scholars [19–22]. In order to make full use of the advantages of polarimetric MIMO radar, Ref. [23] proposed a polarized smoothing generalized multiple signal classification (MUSIC) algorithm based on the generalized MUSIC algorithm, which improved the height measurement accuracy. Based on the MUSIC algorithm [24], Zheng [25] proposed the steering vector synthesis MUSIC algorithm and generalized MUSIC algorithms for the meter-wave polarimetric MIMO radar, which take full advantage of the waveform diversity and polarization diversity with good estimation accuracy and without decoherence processing.

The paper proposes the idea of matrix reconstruction as well as the operation of real-value processing to further improve the estimation accuracy and reduce the computational complexity. The work is motivated to improve the angle estimation accuracy with reduced computational complexity. The problem of the existing algorithms is that the improvement of the angle measurement accuracy and the amount of calculations are contradictory and cannot be unified. The challenges of the topic are to better apply and combine these technologies.

In order to make better use of the advantages of polarimetric MIMO radar, we first analyze the signal model of meter wave polarimetric MIMO radar in the low-elevation area and then study a method based on matrix reconstruction without any prior information. By taking full advantage of the waveform diversity and polarization diversity advantages of the polarimetric MIMO radar, the proposed method has good accuracy at the case of low snapshots or a low signal-to-noise ratio (SNR).

Finally, the proposed algorithm is further analyzed through computer simulation results, and then the correctness and advantages of the proposed algorithm are verified after comparison with the existing algorithms. The innovation of this paper is to apply the polarization MIMO radar to the height measurement of complex terrain. The matrix reconstruction in this paper does not require the prior information of the terrain, and the real value technology can improve the accuracy of height measurement and reduce the amount of calculation.

Notations: Superscript $(\cdot)^*$, $(\cdot)^T$ and $(\cdot)^H$ denote conjugate, transpose and conjugate transpose, respectively. $\otimes$ denotes Kronecker product, respectively. $\boldsymbol{I}_M$ is an identity matrix with dimension M. $\boldsymbol{\Pi}$ is the exchange matrix with ones on its anti-diagonal and zeros elsewhere. $\det(\cdot)$ denotes the matrix determinant.

2. Signal Model of Meter Wave Polarimetric MIMO Radar in Low Elevation Area

The schematic diagram of the polarimetric MIMO radar is shown in Figure 1. The transceiver antennas are all vertically placed with polarization sensitive antenna, and its adjust sensor spacing equals $d_t = d_r = \frac{\lambda}{2}$, where λ is the wavelength. θ_d is the direct wave angle, θ_s is the reflection angle, h_a is the height of the array, and h_t is the height of the target.

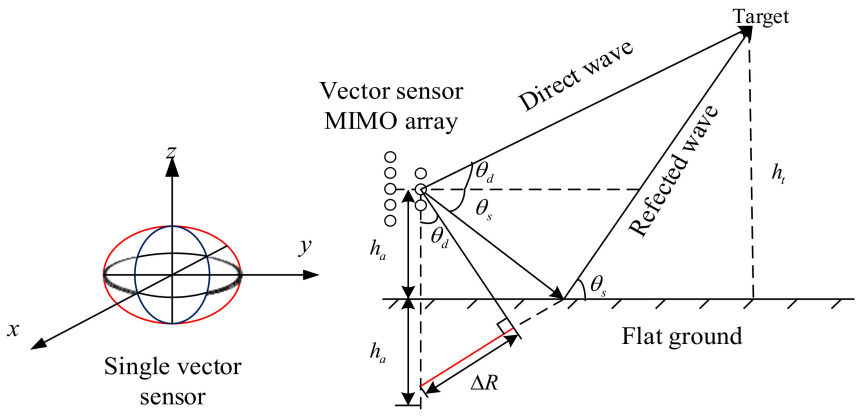

Figure 1. Signal model of meter wave polarimetric MIMO radar in a low-elevation area.

There are M vector sensors in the polarimetric MIMO radar. The transmitted signals of polarimetric MIMO radar are assumed to be a set of orthogonal signals $\boldsymbol{S} = \left[\boldsymbol{S}_1^T, \ldots, \boldsymbol{S}_M^T\right]^T \in \boldsymbol{C}^{6M\times 1}$, where $\boldsymbol{S}_m = [s_{m,1}, \ldots, s_{m,6}]^T$, which satisfies the following Equation (1).

$$s_{m,p}^* s_{n,q} = \begin{cases} P, & m = n \text{ and } p = q \\ 0, & otherwise \end{cases} ; m, n = 1, \ldots M;\ p, q = 1, \ldots, 6. \tag{1}$$

Assuming that the low elevation reflection area is smooth and flat ground, the signal of lth snapshot reaching at the target can be represented as

$$x(l) = [\boldsymbol{b}_t(\theta_d) + \mathrm{e}^{-\mathrm{j}\delta}\rho_h \boldsymbol{b}_t(\theta_s)]^{\mathrm{T}} \boldsymbol{S} \tag{2}$$

where $\delta = \frac{4\pi h_q h_t}{R\lambda}$ is the phase difference due to the range difference of wave propagation between the direct wave and reflected wave, R is the distance between the projection of the target on the ground and the radar, and ρ_h is the Fresnel reflection coefficient of the horizontally polarized wave with a value of

$$\rho_h = \frac{\sin\theta_d - \sqrt{\varepsilon - \cos^2\theta_d}}{\sin\theta_d + \sqrt{\varepsilon - \cos^2\theta_d}} \tag{3}$$

where ε is the surface complex dielectric constant, which can be represented by the relative dielectric constant ε_r and the surface material conductivity σ_e: $\varepsilon = \varepsilon_r - \mathrm{j}60\lambda\sigma_e$.$\boldsymbol{b}(\theta)$ is the whole steering vector, which equals $\boldsymbol{b}(\theta) = \boldsymbol{a}(\theta) \otimes \boldsymbol{g}(\theta)$, where $\boldsymbol{a}(\theta)$ is the spacial steering vector and $\boldsymbol{g}(\theta)$ is the polarization steering vector of a single electromagnetic vector sensor, which can be expressed as:

$$\boldsymbol{a}(\theta) = [1, \exp(-\mathrm{j}\pi\sin(\theta)), \cdots, \exp(-\mathrm{j}(M-1)\pi\sin(\theta))]^{\mathrm{T}} \tag{4}$$

$$\boldsymbol{g}(\theta) = \begin{bmatrix} \cos\phi\cos\theta & -\sin\phi \\ \sin\phi\cos\theta & \cos\phi_k \\ -\sin\theta & 0 \\ -\sin\phi & -\cos\phi\cos\theta \\ \cos\phi & -\sin\phi\cos\theta \\ 0 & \sin\theta \end{bmatrix} \begin{bmatrix} \sin\gamma e^{j\eta} \\ \cos\gamma \end{bmatrix} \tag{5}$$

where θ represents θ_d or θ_s, and $\boldsymbol{b}_r(\theta) = \boldsymbol{b}_t(\theta)$. Therefore, we can obtain the values of $\boldsymbol{b}_r(\theta_d), \boldsymbol{b}_r(\theta_s), \boldsymbol{b}_t(\theta_d), \boldsymbol{b}_t(\theta_s)$. As elevation measurement is the primary purpose of this paper, we set the azimuth as $\phi = 90^\circ$. Data for the lth snapshot received by the entire array can be expressed as

$$\boldsymbol{X}(l) = [\boldsymbol{b}_r(\theta_d) + \mathrm{e}^{-\mathrm{j}\delta}\rho_h \boldsymbol{b}_r(\theta_s)]\xi(l)[\boldsymbol{b}_t(\theta_d) + \mathrm{e}^{-\mathrm{j}\delta}\rho_h \boldsymbol{b}_t(\theta_s)]^{\mathrm{T}} \boldsymbol{S} + \boldsymbol{N}(l) \tag{6}$$

where $\xi(l)$ is the complex reflection coefficient, and $\boldsymbol{N}(l)$ is the Gaussian white noise, with a mean of zero and a variance of σ^2. The following formula can be obtained after matching filtering using the transmitted signals to Equation (6):

$$\boldsymbol{Y}(l) = [\boldsymbol{b}_r(\theta_d) + \mathrm{e}^{-\mathrm{j}\delta}\rho_h \boldsymbol{b}_r(\theta_s)]\xi(l)[\boldsymbol{b}_t(\theta_d) + \mathrm{e}^{-\mathrm{j}\delta}\rho_h \boldsymbol{b}_t(\theta_s)]^{\mathrm{T}} + \boldsymbol{N}(l)\boldsymbol{S}^H(l) \tag{7}$$

For Equation (7), the received data under the lth snapshot can be expressed as the following formula,

$$\boldsymbol{Y} = [\boldsymbol{b}_t(\theta_d) + \mathrm{e}^{-\mathrm{j}\delta}\rho_h \boldsymbol{b}_t(\theta_s)] \otimes [\boldsymbol{b}_r(\theta_d) + \mathrm{e}^{-\mathrm{j}\delta}\rho_h \boldsymbol{b}_r(\theta_s)]\xi(l) + \boldsymbol{N} \in \boldsymbol{C}^{36MN \times L} \tag{8}$$

According to the conclusion of Ref. [21], the noise of $\boldsymbol{N}$ is still Gaussian white noise after matching filtering and vectorization operation.

3. Real Valued MUSIC Height Measurement Method Based on Matrix Reconstruction

To solve the problem of the effect of the multi-path reflection echo signal in the low-elevation area of the polarimetric MIMO radar, this section reconstructs the received signal data Equation (8) as matrix $\boldsymbol{Z}(l) \in \boldsymbol{C}^{MM \times 36}$, which can be expressed as the following equation:

$$\boldsymbol{Z}(l) = [\boldsymbol{Y}_{1,1}(l), \ldots, \boldsymbol{Y}_{1,M}(l), \boldsymbol{Y}_{2,1}(l), \ldots, \boldsymbol{Y}_{M,M}(l)] \tag{9}$$

where $\boldsymbol{Y}_{m,n}(l) \in \boldsymbol{C}^{36\times 1}$ represents the data received by the nth vector sensor and the mth transmitted signal. Equation (9) can be expanded as the following formula:

$$\boldsymbol{Z}(l) = \boldsymbol{A}\Lambda_{\xi}(l)\boldsymbol{G} + \boldsymbol{V}(l) = \boldsymbol{A}\boldsymbol{D}(l) + \boldsymbol{V}(l) \tag{10}$$

where $\boldsymbol{A}$ is the steering vector after the matrix reconstruction, $\boldsymbol{V}(l)$ is the noise matrix of the reconstructed data, $\boldsymbol{G}$ contains all the polarization information of the received data, and $\Lambda_{\xi}(l)$ includes the reflection coefficient, the range difference of wave propagation and other information as follows.

$$\boldsymbol{A} = \begin{bmatrix} \boldsymbol{a}_r(\theta_d) \otimes \boldsymbol{a}_t(\theta_d) & \boldsymbol{a}_r(\theta_d) \otimes \boldsymbol{a}_t(\theta_s) \\ \boldsymbol{a}_r(\theta_s) \otimes \boldsymbol{a}_t(\theta_d) & \boldsymbol{a}_r(\theta_s) \otimes \boldsymbol{a}_t(\theta_s) \end{bmatrix} \in \boldsymbol{C}^{MM\times 4} \tag{11}$$

$$\boldsymbol{G} = \begin{bmatrix} \boldsymbol{g}(\theta_d) \otimes \boldsymbol{g}(\theta_d) & \boldsymbol{g}(\theta_d) \otimes \boldsymbol{g}(\theta_s) \\ \boldsymbol{g}(\theta_s) \otimes \boldsymbol{g}(\theta_d) & \boldsymbol{g}(\theta_s) \otimes \boldsymbol{g}(\theta_s) \end{bmatrix}^{T} \in \boldsymbol{C}^{4\times 36} \tag{12}$$

$$\Lambda_{\xi}(l) = diag\left\{\xi(l), \mathrm{e}^{-\mathrm{j}\delta}\rho_h\xi(l), \mathrm{e}^{-\mathrm{j}\delta}\rho_h\xi(l), \mathrm{e}^{-\mathrm{j}2\delta}\rho_h^2\xi(l)\right\} \tag{13}$$

After observation, it is not difficult to find that the column of $\boldsymbol{G}$ is linear independent and, when $\xi(l) \neq 0$, $\boldsymbol{R}_D = E\left(\boldsymbol{D}(l)\boldsymbol{D}(l)^H\right)$, has rank $\min(4, 36) = 4$. Furthermore, it is important to note that, in Equation (10), when the rank of $\boldsymbol{A}$ is 4, the rank loss generated by the multipath coherence signal has been resolved, i.e., the matrix reconstruction method eliminates the effect of the multipath coherence signal. With K noncoherent low elevation targets, the proposed method can solve the multipath coherent rank loss phenomenon for, at most, $36/4$.

However, the values in Equation (10) are complex values, and thus direct low-elevation estimation leads to greater computational complexity. To reduce the algorithm complexity, we perform the real-value processing using the unitary matrix with Equation (10) and derive the corresponding real-value MUSIC elevation estimation method.

When the received data has L snapshots, the corresponding data expression of $\boldsymbol{Z}_L = [\boldsymbol{Z}(1), \ldots, \boldsymbol{Z}(L)] \in \boldsymbol{C}^{MM\times 36L}$ can be obtained by Equation (10). To make full use of the conjugated data, Z_L can be extended as

$$\boldsymbol{Z}_{L,U} = [\boldsymbol{Z}_L, \boldsymbol{\Pi}_{MM}\boldsymbol{Z}_L^*\boldsymbol{\Pi}_{36L}] \in \boldsymbol{C}^{MM\times 72L} \tag{14}$$

where $\boldsymbol{\Pi}_N$ is a commutative matrix with 1 on the antidiagonal elements and the remaining position elements of 0. We can easily verify that $\boldsymbol{Z}_{L,U}$ is the centrosymmetric Hermite matrix [26], and the real-valued matrix can be obtained by processing with Equation (14) using the unitary matrix [27].

$$\boldsymbol{Z}_R = \boldsymbol{\Gamma}_{MM}^H\boldsymbol{Z}_{(k)}\boldsymbol{\Gamma}_{72L} \tag{15}$$

where $\boldsymbol{\Gamma}_K$ is a sparse unitary matrix, whose odd and even dimensions are defined as, respectively:

$$\begin{cases} \boldsymbol{\Gamma}_{2K+1} = \frac{1}{\sqrt{2}}\begin{bmatrix} \boldsymbol{I}_K & 0_{K\times 1} & j\boldsymbol{I}_K \\ 0_{1\times K} & \sqrt{2} & 0_{1\times K} \\ \boldsymbol{\Pi}_K & 0_{K\times 1} & -j\boldsymbol{\Pi}_K \end{bmatrix} \\ \boldsymbol{\Gamma}_{2K} = \frac{1}{\sqrt{2}}\begin{bmatrix} \boldsymbol{I}_K & j\boldsymbol{I}_K \\ \boldsymbol{\Pi}_K & -j\boldsymbol{\Pi}_K \end{bmatrix} \end{cases} \tag{16}$$

When the number of dimension of received data is large, the huge calculation amount will increase the practical application difficulty. In order to reduce the dimension of the receiving data, and to reduce the impact of the noise on the data, we can use Singular Value Decomposition (SVD) technology to handle Equation (15), as follows:

$$\boldsymbol{Z}_R = \boldsymbol{U}_s\boldsymbol{\Lambda}_s\boldsymbol{V}_s^H + \boldsymbol{U}_n\boldsymbol{\Lambda}_n\boldsymbol{V}_n^H \in \boldsymbol{C}^{MM\times 72L} \tag{17}$$

As there are four transmission paths in the low elevation region for one target and the reconstructed data covariance matrix rank is 4; therefore, $\boldsymbol{U}_s \in \boldsymbol{C}^{MN\times 4}$ and $\boldsymbol{U}_n \in \boldsymbol{C}^{MN\times MN-4}$ are composed of left singular value vectors corresponding to four large singular values and left singular values corresponding to $MN-4$ small singular values. $\boldsymbol{\Lambda}_s$ and $\boldsymbol{\Lambda}_n$ consist of four large singular values and the remaining $MN-4$ large singular values. Similarly, $\boldsymbol{V}_s \in \boldsymbol{C}^{72L\times 4}$ and $\boldsymbol{V}_n \in \boldsymbol{C}^{72L\times MN-4}$ consists of right singular value vectors corresponding to four large singular values and a vector of right singular values corresponding to $MN-4$ small singular values. Equation (15) right is multiplied with $\boldsymbol{V}_s$, and then we have

$$\widetilde{\boldsymbol{Z}}_R = \boldsymbol{Z}_R \boldsymbol{V}_s \in \boldsymbol{C}^{MN\times 4} \tag{18}$$

According to Equation (18), the dimension of matrix $\boldsymbol{Z}_R$ decreases from $72L$ to 4. It is not difficult to find $72L \gg 4$ when the number of snapshots L is large, and thus it is not difficult to prove that singular value techniques can greatly reduce the matrix dimension.

In the same way, the covariance matrix of the real-valued data can be obtained by the following equation:

$$\boldsymbol{R}_{Z_R} = \frac{1}{72L}\widetilde{\boldsymbol{Z}}_R\widetilde{\boldsymbol{Z}}_R^H \in \boldsymbol{C}^{MM\times MM} \tag{19}$$

Eigenvalue decomposition of matrix $\boldsymbol{R}_{Z_R}$ yields the following formula.

$$\boldsymbol{R}_{Z_R} = \boldsymbol{E}_s\boldsymbol{\Lambda}_s\boldsymbol{E}_s^H + \boldsymbol{E}_n\boldsymbol{\Lambda}_n\boldsymbol{E}_n^H \tag{20}$$

Matrices $\boldsymbol{E}_s$ and $\boldsymbol{E}_n$ represent the signal and noise subspaces, respectively, whose eigenvalues constitute the diagonal matrices $\boldsymbol{\Lambda}_s$ and $\boldsymbol{\Lambda}_n$. Since $\boldsymbol{R}_{Z_R}$ is a real-valued matrix, both $\boldsymbol{E}_s$ and $\boldsymbol{E}_n$ are real-valued matrices. Based on the orthogonality of the signal subspace and noise subspace, the following spectrum formula can be obtained.

$$P(\theta_d, \theta_s) = \frac{\det\left(\boldsymbol{E}_n^H\boldsymbol{E}_n\right)}{\det\left(\boldsymbol{A}_R^H\boldsymbol{E}_n\boldsymbol{E}_n{}^{\mathrm{H}}\boldsymbol{A}_R\right)} \tag{21}$$

Equation (21) is called the generalized MUSIC algorithm. The difference between it and the traditional MUSIC algorithm is that there is no need for information of the steering vector. It is sufficient to know the steering matrix because the steering matrix is orthogonal to the noise subspace and because the angle estimation can be obtained by using this point.

As the received data is processed as real-valued data by the unitary matrix, the steering vector $\boldsymbol{A}_R = \Gamma_{M^2}^H\boldsymbol{A}$ for the spectral peak search in Equation (21) does not contain any polarization parameter, the range difference of wave propagation and reflection coefficient information; thus, it is not difficult to prove that the proposed method can estimate the target elevation value without the polarization information.

The above equation is a two-dimensional spectral peak search, which can be reduced to a one-dimensional search according to the relationship between the angle of direct wave and the reflected wave as shown below

$$\theta_s = -\arctan(\tan\theta_d + 2h_a/R) \tag{22}$$

Based on the distance R and elevation estimations, the height of the target can be calculated as:

$$H \approx R\sin\theta_d + h_a \tag{23}$$

4. Summary and Computational Complexity of the Proposed Algorithm

The algorithm steps studied in this paper are as follows:

1. Reconstruct the received signal data using Equation (9).
2. The unitary matrix is used to process the real-value of the reconstructed received signal matrix.

3. Reduce the effect of big dimension of received data and noise using the singular value technique.
4. The signal covariance matrix was obtained by Equation (19), and then the eigenvalue was decomposed to obtain the noise subspace matrix.
5. According to the noise subspace matrix, the spectral peak search was performed as in Equation (21).
6. The target height is obtained according to the geometric relationship of Equation (23).

According to the algorithm steps, it is not difficult to find that the complexity of the proposed method is mainly divided into the following parts: (1) real-valued processing; (2) estimate the real-valued covariance matrix; (3) eigenvalue decomposition of the covariance; and (4) spectral peak search. The specific expression is as follows: (1) $24 \cdot 72M^2L$; (2) $72M^4L$; (3) M^6; (4) $num \cdot \left(8M^4 + 36M^2\right)$. Therefore, the complexity of the proposed algorithm is $36M^2(48L + num) + M^4(72L + 8num) + M^6$.

The generalized MUSIC algorithm proposed in Ref. [28] is abbreviated as G-MUSIC; the generalized MUSIC algorithm applied in polarimetric MIMO radar is abbreviated as PG-MUSIC [23]; the height measurement method of maximum likelihood estimation proposed in Ref. [29] is abbreviated as the ML algorithm; and its extension algorithm in polarimetric MIMO radar is abbreviated as P-ML [25]. The G-MUSIC algorithm complexity is $4M^4L + 4M^6 + 4\Theta\left(32M^2 + 8M^4\right)$.

The complexity of PG-MUSIC algorithm is $4\left(36M^2\right)^3 + 4\left(36M^2\right)^2L + 4\Theta\left(36 \cdot 32\mathrm{M}^2 + 8 \cdot 36^2M^4\right)$. The complexity of ML algorithm is $4M^4\left(L + M^2\right) + 4\Theta\left(32M^2 + 4M^4 + M^6\right)$. The complexity of P-ML algorithm is $4 \cdot 36^2M^4\left(L + 36M^2\right) + 4\Theta\left(36^3M^6 + 32 \cdot 36M^2 + 4 \cdot 36^2M^4\right)$.

5. Computer Simulation Results

This section verifies the reliability and superiority of the proposed algorithm mainly through simulation experiments. In this paper, the angle search range is set as $0.5^\circ - 12^\circ$, the search angle interval is 0.01°, and the number of searches is 1151. A meter-wave polarimetric MIMO radar system has the transceiver array elements $M = N = 6$, and the adjusted element spacing is $d_t = d_r = \lambda/2$. In addition, the wavelength is set as $\lambda = 1$. The height array is $h_a = 5m$, and number of Monte Carlo experiments is $K = 500$. In simulation experiments, the number of target is set to 1, and the root mean square error is defined as

$$\mathrm{RMSE\_DOA} = \sqrt{\frac{1}{K}\sum_{k=1}^{K}\left(\hat{\theta}_k - \theta_d\right)^2} \tag{24}$$

$$\mathrm{RMSE\_H} = \sqrt{\frac{1}{K}\sum_{k=1}^{K}\left(\hat{H}_k - h_t\right)^2} \tag{25}$$

where $\hat{\theta}_k$ is the estimated elevation value obtained by the kth experiment, $\hat{H}_k$ is the estimated target height obtained by the kth experiment, and K is the number of Monte Carlo experiments.

Example 1: In this experiment, the number of $L = 10$, the actual elevation of the target is 3°. The SNR is set as 10 dB. Figure 2 is a spatial spectrum of the proposed method with 10 times. It can be seen from Figure 2 that the proposed method can correctly measure the target elevation angle, which proves the correctness of the proposed method.

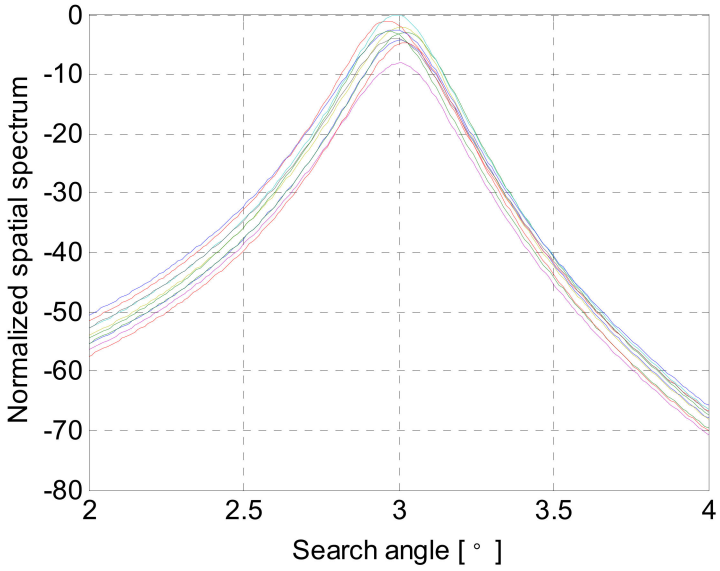

Figure 2. The spatial spectrum of the proposed algorithm with 10 times.

Example 2: In this experiment, the number of snapshots is $L = 10$, the actual elevation of the target is 3°, the distance between the target and the radar is R = 200 km, and the range of SNR is from -10 to 10 dB. Figure 3 shows the relationship between the RMSE of angle estimation and SNR for the five algorithms, and Figure 4 shows the RMSR of height measurement and SNR of the five algorithms.

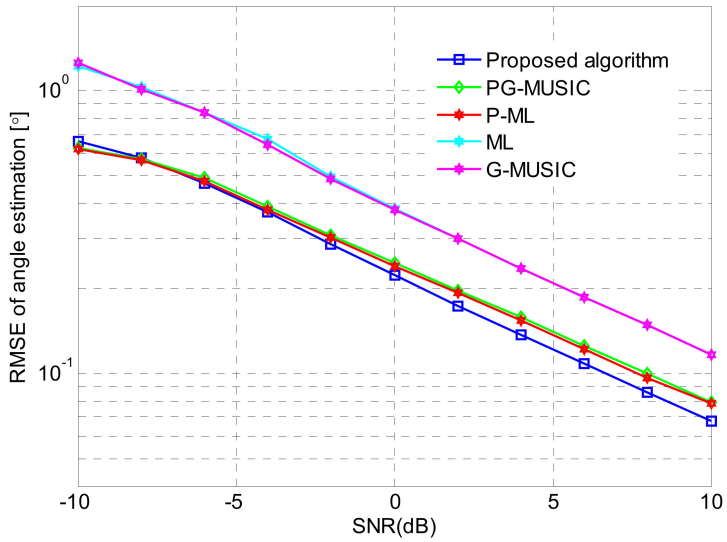

Figure 3. RMSE of angle estimation versus SNR.

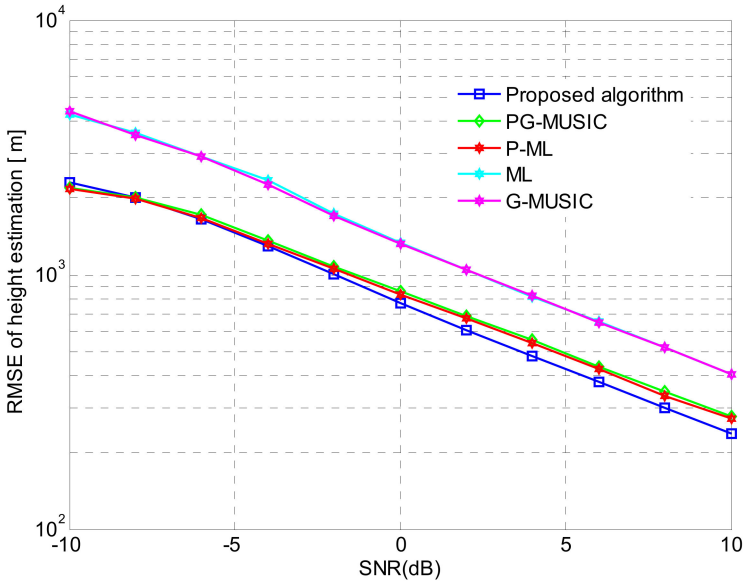

Figure 4. RMSE of height measurement versus SNR.

From Figures 3 and 4, the PG-MUSIC and P-ML methods show better estimation accuracy than the G-MUSIC and ML methods, which demonstrates the polarization diversity advantage of polarizing-sensitive arrays. Moreover, the proposed algorithm outperforms the PG-MUSIC and P-ML methods, which demonstrates the superiority of the proposed algorithm.

Example 3: Figure 5 shows the relationship between the computational complexity and the number of array elements of the five algorithms. It can be found from Figure 5 that the computational complexity of the PG-MUSIC and P-ML methods is significantly higher than that for the G-MUSIC and ML methods. This indicates that, although polarimetric MIMO radar has a polarization diversity advantage, it also increases the algorithmic computational complexity.

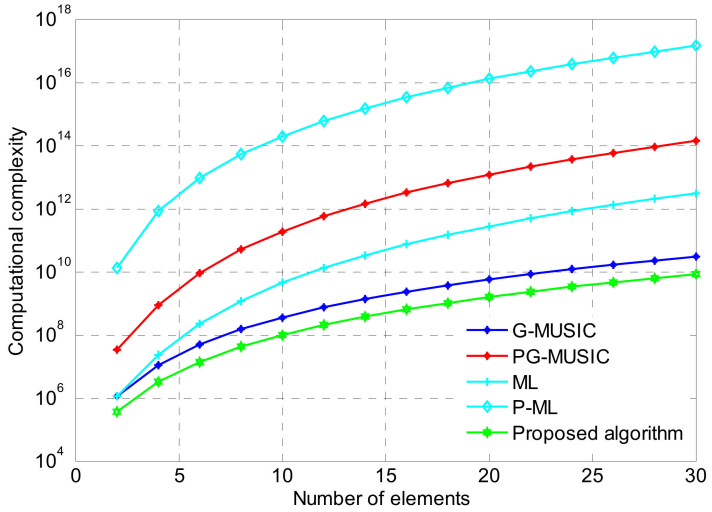

Figure 5. Complexity changes with the array number.

Notably, the proposed algorithm has the lowest computational complexity because of the data with real values and because the steering vector dimension for spectrum search is lower than for the PG-MUSIC and P-ML methods. This proves that the proposed method is more conducive to engineering implementations. In addition, according to the experimental results of this example and example 2, compared with the other four

algorithms, the proposed algorithm reduces the computing complexity and improves the accuracy of the target elevation and height measurement.

6. Conclusions

To further improve the measurement accuracy, we studied a height measurement method based on the meter-wave polarimetric MIMO radar, which makes full use of the waveform diversity and polarization diversity. First, the receiving signal model was analyzed. According to the height measurement signal model, the received data matrix was reconstructed to eliminate the effect of the multipath reflection echo. To reduce the algorithm complexity, the reconstructed data matrix was processed with real values using a unitary matrix.

Finally, the corresponding spectrum search was presented, which requires no known polarization information. In the simulation experiment, the proposed algorithm was comprehensively compared with the state-of-the-art algorithms, which showed that the proposed algorithm had the best performance. Therefore, when selecting the estimation algorithms, we can consider using the real value processing technology in this paper to improve the diversity of samples. In addition, the decoherence method of matrix reconstruction is a good decoherence method that does not depend on the information of the terrain.

Author Contributions: Conceptualization, G.Z. and C.C.; methodology, G.Z.; software, G.Z.; writing—original draft preparation, Y.S.; writing—review and editing, C.C. All authors have read and agreed to the published version of the manuscript.

Funding: This work was supported by National Natural Science Foundation of China under Grant 61971438.

Data Availability Statement: The data can be obtained by sending an email to zheng-gm@163.com.

Conflicts of Interest: The authors declare no conflict of interest.

References

1. Li, J.; Stoica, P. MIMO Radar with Collocated Antennas. *IEEE Signal Process. Mag.* **2007**, *24*, 106–114. [CrossRef]
2. Liu, Y.B.; Wang, C.Y.; Gong, J.; Tan, M.; Chen, G. Robust suppression of deceptive jamming with VHF-FDA-MIMO radar under multipath effects. *Remote Sens.* **2022**, *14*, 942. [CrossRef]
3. Luo, J.; Zhang, Y.; Yang, J.; Zhang, D.; Zhang, Y.; Zhang, Y.; Huang, Y.; Jakobsson, A. Online sparse DOA estimation based on sub–aperture recursive LASSO for TDM–MIMO radar. *Remote Sens.* **2022**, *14*, 2133. [CrossRef]
4. Zheng, G.; Wu, B.; Ma, Y.; Chen, B. DOA Estimation with a sparse uniform array of orthogonally oriented and spatially separated dipole-triads. *IET Radar Sonar Navig.* **2014**, *8*, 885–894. [CrossRef]
5. Zheng, G. Two-dimensional DOA estimation for polarization sensitive array consisted of spatially spread crossed-dipole. *IEEE Sens. J.* **2018**, *18*, 5014–5023. [CrossRef]
6. Wong, K.T.; Yuan, X. "Vector cross-product direction-finding" with an electromagnetic vector-sensor of six orthogonally oriented but spatially noncollocating dipoles/loops. *IEEE Trans. Signal Process.* **2011**, *59*, 160–171. [CrossRef]
7. Song, Y.; Wong, K.T.; Yuan, X. Correction to "Vector cross-product direction-finding" with an electromagnetic vector-sensor of six orthogonally oriented but spatially noncollocating dipoles/loops. *IEEE Trans. Signal Process.* **2014**, *62*, 1028–1030. [CrossRef]
8. Wong, K.T.; Song, Y.; Fulton, C.J.; Khan, S.; Tam, W.Y. Electrically "Long" Dipoles in a collocated/orthogonal triad—For direction finding and polarization estimation. *IEEE Trans. Antennas Propag.* **2017**, *65*, 6057–6067. [CrossRef]
9. Khan, S.; Wong, K.T.; Song, Y.; Tam, W.Y. Electrically large circular loops in the estimation of an incident emitter's direction-of-arrival or polarization. *IEEE Trans. Antennas Propag.* **2018**, *66*, 3046–3055. [CrossRef]
10. Khan, S.; Wong, K.T. A six component vector comprising electrically long dipoles and large loops –to simultaneously estimate incident sources' direction of arrival and polarizations. *IEEE Trans. Antennas Propag.* **2020**, *68*, 6355–6363. [CrossRef]
11. Guo, Y.; Hu, X.; Feng, W.; Gong, J. Low-Complexity 2D DOA Estimation and Self-Calibration for Uniform Rectangle Array with Gain-Phase Error. *Remote Sens.* **2022**, *14*, 3064. [CrossRef]
12. Mao, Z.; Liu, S.; Qin, S.; Haung, Y. Cramér-Rao Bound of joint DOA-range estimation for coprime frequency diverse arrays. *Remote Sens.* **2022**, *14*, 583. [CrossRef]
13. Liu, Y.; Liu, H. Target Height Measurement under Complex Multipath Interferences without Exact Knowledge on the Propagation Environment. *Remote Sens.* **2022**, *14*, 3099. [CrossRef]
14. Zheng, G.; Song, Y. Signal model and method for joint angle and range estimation of low-elevation target in meter-wave FDA-MIMO radar. *IEEE Commun. Lett.* **2022**, *26*, 449–453. [CrossRef]

15. Song, Y.; Hu, G.; Zheng, G. Height measurement with meter wave MIMO radar based on precise signal model under complex terrain. *IEEE Access* **2021**, *9*, 49980–49989. [CrossRef]
16. Chen, C.; Tao, J.; Zheng, G.; Song, Y. Meter-wave MIMO radar height measurement method based on adaptive beamforming. *Digit. Signal Process.* **2022**, *120*, 103272. [CrossRef]
17. Chen, C.; Tao, J.; Zheng, G.; Song, Y. Beam split algorithm for height measurement with meter-wave MIMO radar. *IEEE Access* **2021**, *9*, 5000–5010. [CrossRef]
18. Wang, H.; Zheng, G.; Liu, Y.; Song, Y. Low elevation and range joint estimation method with meter wave FDA-MIMO radar based on sparse array. *IET Radar Sonar Navig.* **2022**, *16*, 1179–1187. [CrossRef]
19. Jiang, H.; Zhang, J.-K.; Wong, K.M. Joint DOD and DOA Estimation for Bistatic MIMO Radar in Unknown Correlated Noise. *IEEE Trans. Veh. Technol.* **2015**, *64*, 5113–5125. [CrossRef]
20. Chintagunta, S.; Ponnusamy, P. Integrated polarisation and diversity smoothing algorithm for DOD and DOA estimation of coherent targets. *IET Signal Process.* **2018**, *12*, 447–453. [CrossRef]
21. Wen, F.; Shi, J.; Zhang, Z. Joint 2D-DOD, 2D-DOA And Polarization Angles Estimation for Bistatic EMVS-MIMO Radar Via PARAFAC Analysis. *IEEE Trans. Veh. Technol.* **2020**, *29*, 1626–1638. [CrossRef]
22. Wang, X.; Wan, L.; Huang, M.; Shen, C.; Zhang, K. Polarization channel estimation for circular and non-circular signals in massive MIMO systems. *IEEE J. Sel. Top. Signal Process.* **2019**, *13*, 1001–1016. [CrossRef]
23. Tan, J.; Nie, Z. Polarization Smoothing Generalized MUSIC algorithm with PSA monostatic MIMO radar for low angle estimation. *Electron. Lett.* **2018**, *54*, 527–529. [CrossRef]
24. Stoica, P.; Nehorai, A. MUSIC, maximum likelihood, and Cramer-Rao bound. *IEEE Trans. Acoust. Speech Signal Process.* **1989**, *37*, 720–741. [CrossRef]
25. Zheng, G.; Song, Y.; Chen, C. Height Measurement for with wave polarimetric MIMO radar: Signal model and MUSIC algorithm. *Signal Process.* **2022**, *190*, 108344. [CrossRef]
26. Ding, J.C.; Chen, H.W.; You, B.; Li, X.; Zhuang, Z.W. Fluctuating target detection in low-grazing angle with Multi-input Multiple-output radar. In Proceedings of the 2012 IEEE 11th International Conference on Signal Processing, Beijing, China, 21–25 October 2012; IEEE: Piscataway, NJ, USA, 2013.
27. Li, J.; Jiang, D.; Zhang, X. DOA Estimation Based on Combined Unitary ESPRIT for Coprime MIMO Radar. *IEEE Commun. Lett.* **2017**, *21*, 96–99. [CrossRef]
28. Haimovich, A.M.; Blum, R.S.; Cimini, L.J. MIMO Radar with Widely Separated Antennas. *IEEE Signal Process. Mag.* **2007**, *25*, 116–129. [CrossRef]
29. Rahamim, D.; Tabrikian, J.; Shavit, R. Source localization using vector sensor array in a multipath environment. *IEEE Trans. Signal Process.* **2004**, *52*, 3096–3103. [CrossRef]